Lawrence Berkeley National Laboratory
Recent Work

Title
Correspondence between Microwave and Submillimeter Absorptivity in Epitaxial Thin Films of YBa{sub 2}Cu{sub 3}O{sub 7}

Permalink
https://escholarship.org/uc/item/6650x3mf

Journal
Physical Review B, 47(13)

Authors
Miller, D.
Richards, P.L.
Etemad, S.
et al.

Publication Date
1991-11-01
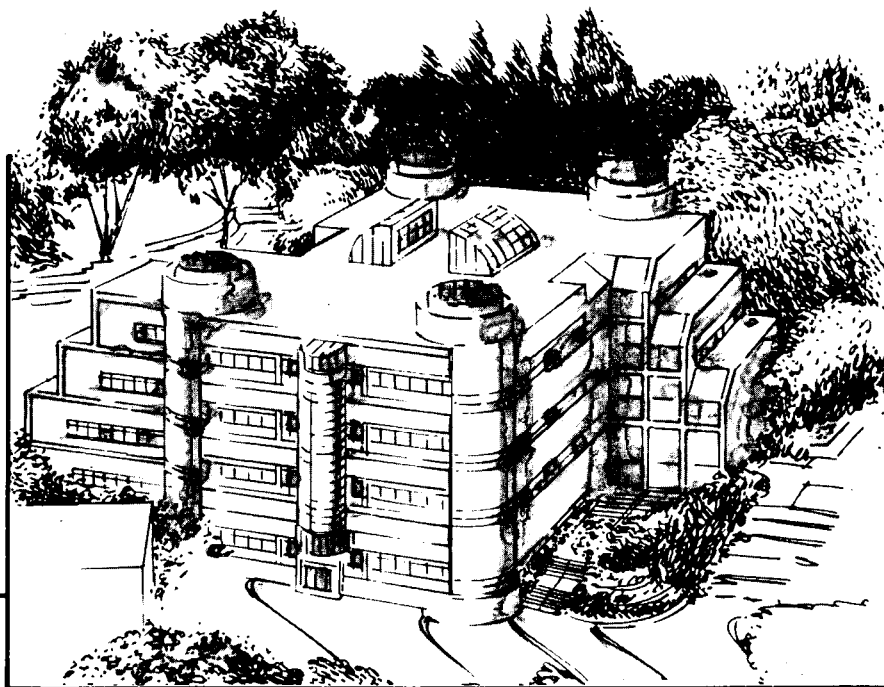
Center for Advanced Materials

CAM

Correspondence between Microwave and Submillimeter Absorptivity in Epitaxial Thin Films of $YBa_2Cu_3O_7$

D. Miller, P.L. Richards, S. Etemad, A. Inam, T. Venkatesan, B. Dutta, X.D Wu, C.B. Eom, T.H. Geballe, N. Newman, and B.F. Cole

November 1991

Materials and Chemical Sciences Division

Lawrence Berkeley Laboratory • University of California

ONE CYCLOTRON ROAD, BERKELEY, CA 94720 • (415) 486-4755

DISCLAIMER

DISCLAIMER

Correspondence between Microwave and Submillimeter Absorptivity in Epitaxial Thin Films of YBa$_2$Cu$_3$O$_7$

D. MILLER, P.L. RICHARDS

Department of Physics, University of California, and Materials Sciences Division, Lawrence Berkeley Laboratory,Berkeley CA 94720

S. ETEMAD, A. INAM, T. VENKATESAN, B. DUTTA, X.D. WU

Bell Communications Research, Red Bank, New Jersey 07701

C.B. EOM, T.H. GEBALLE

Department of Applied Physics, Stanford University, Stanford CA 94305

N. NEWMAN, B.F. COLE

Conductus, Inc., Sunnyvale, CA 94086

PACS Nos. 74.30.Gn, 74.70.Vy, 74.75.+t, 07.62.+s

Abstract

We have measured the low temperature loss in six epitaxial a-b plane films of the high-T_c superconductor $YBa_2Cu_3O_7$. Submillimeter measurements from 25 to 700 cm^{-1} were made at 2K by a novel direct absorption technique in which the film acts as the absorbing element in a composite bolometric detector. Microwave measurements near 10 GHz (0.3 cm^{-1}) were made on five of the same films by resonance techniques at 4K. The ~0.4μm thick films were grown epitaxially on $SrTiO_3$, $LaAlO_3$ and MgO by off-axis sputtering and laser deposition. The absorptivities measured for all films studied are qualitatively similar, increasing smoothly with frequency, with no gap-like features below the well known absorption edge at 450 cm^{-1}. We use a two-fluid model and a model of weakly coupled grains to fit the data below 450 cm^{-1} for each film. When the penetration depth determined from muon spin rotation measurements is used to constrain each model, the weakly coupled grain model is able to fit the measured absorptivities for all films, but the two-fluid model is less successful. In addition, results from a Kramers-Kronig analysis of the loss data are in remarkable agreement with the weakly coupled grain model best fits for each film.

I. Introduction

A knowledge of the loss at microwave, millimeter and submillimeter frequencies plays an important role in our understanding of the superconducting state properties of high-T_c superconductors such as $YBa_2Cu_3O_7$. These measurements, however, are complicated by several factors, including the anisotropy and the complex microstructure of these materials. Advances in the technology of materials fabrication have resulted in the ability to study highly oriented samples. In addition, the uniformity of sample quality has improved and

along with it the reproducibility of the resulting optical spectra. However, the interpretation of such measurements remain somewhat controversial, at least in part due to the lack of a consistent picture of the loss spectrum between microwave and submillimeter frequencies.

One of the most studied cuprate superconductors is the $T_c \sim 90$ K material $YBa_2Cu_3O_7$ (YBCO). Almost all submillimeter measurements of a-b plane oriented YBCO observe an onset of absorption at ~450 cm^{-1}.[1-6] While this absorption feature is most prominent at low temperatures there is evidence that it exists above T_c. In addition the onset frequency depends only weakly on temperature and is independent of the T_c of the sample.[2] These observations suggest that this feature is not a conventional superconducting energy gap. At temperatures below ~30 K and for frequencies below ~ 300 cm^{-1} the reflectivity of YBCO is greater than ~98%. Several groups have observed reflectivities which within experimental uncertainties are consistent with unity below ~140 cm^{-1}.[1-3,6,7] Measurements with polarized infrared radiation on untwinned YBCO crystals[8] show that the absorption is anisotropic in the a-b plane. For current flow perpendicular to the Cu-O chains, the absorption below 500 cm^{-1} is much smaller than for current flow along the chains.[8]

Recently several groups have measured the transmittance of thin YBCO films[9,10] in order to obtain more accurate data, especially at frequencies below a few hundred wavenumbers. Despite the complications associated with the optical properties of the substrate these experiments suggest that there is some non-vanishing fraction of normal (absorbing) carriers well below T_c. No gap-like spectral feature is observed in these experiments below 450 cm^{-1}.[9]

Three basic interpretations have been given to the infrared data. Some workers have interpreted the frequency (~ 140 cm^{-1}) at which the reflectivity

becomes unity, within experimental uncertainty, with a superconducting gap.[1-3,6,11,12] For the samples with T_c = 90 K this leads to a value for the gap of 2Δ ≈ 2.2 $k_B T_c$. Others identify the 450 cm⁻¹ feature with the gap,[3,6] giving 2Δ ≈ 7 $k_B T_c$ for samples with T_c = 90 K. Still others attribute the 450 cm⁻¹ feature to a strong electron-phonon interaction[13] and suggest that the relaxation time is short enough in YBCO that no infrared gap should be visible.[1]

Microwave measurements show a temperature dependent component to the loss which is in reasonable agreement with the predictions of Mattis and Bardeen for temperatures near T_c, e.g. T > 80K, plus a substantial residual loss that remains at low temperatures. This residual loss is minimized in high quality epitaxial a-b plane films. Both contributions to the loss vary as frequency squared from ~10 to ~100 GHz.[14]

In this paper we present a novel experimental approach which is used to obtain accurate direct absorptivity data on epitaxial a-b plane films in the frequency range between microwave loss and infrared reflectivity measurements. Data are presented for six high quality oriented films of fully oxygenated YBCO at 2K. There is a significant advantage of a direct absorptivity measurement over reflectivity measurements when the sample reflectivities being studied are close to unity, as occurs for these materials below approximately 300 cm⁻¹. Uncertainties associated with the precise determination of unity reflectivity are minimized by measuring the absorptivity directly. Sources of error which tend to multiply the resulting spectra (e.g., drift, sample placement errors, standing waves) which can dominate the signal for reflectivity or transmissivity measurements are minimized in the absorptivity measurement. Also, direct absorptivity measurements are less sensitive to substrate properties than transmissivity measurements. Since the first

results of our experiment were announced,[15] similar techniques have been used by others to measure absorptivity in single crystals of YBCO.[16]

Along with the submillimeter absorptivity data we present microwave surface resistance measurements made near 10 GHz (0.3 cm^{-1}) and 4K for five of the six films. Using the well documented frequency squared dependence of the microwave loss up to 100 GHz,[14] we can infer the loss in our films over four decades in frequency. The absorptivity varies as frequency squared up to ~ 10 cm^{-1} (300 GHz) and then approaches a constant by 450 cm^{-1} where there is a sharp onset of additional absorption. Other investigators have explored the relationship between the residual microwave loss and the submillimeter absorptivity deduced from reflectivity measurements. Our data are generally consistent with early work,[17] but not with a recent paper which shows higher microwave losses relative to the infrared loss than we observe.[5]

The data from all films are compared with a fitting function which has three parameters. These parameters can be interpreted either in terms of a homogeneous two-fluid model or in terms of an inhomogeneous weakly coupled grain model of the YBCO film. Satisfactory fits can be obtained from the weakly coupled grain model when one of the parameters is constrained by the accepted value of the superconducting penetration depth deduced from muon spin rotation (μsr) measurements. The complex conductivity $\sigma(\omega)$ is also calculated from the Kramers-Kronig (KK) transform of the loss data for each sample. This analysis is consistent with the results of other workers[1-6] above ~400 cm^{-1}. Below ~400 cm^{-1} where our new data play an important role, the results of this analysis are in excellent agreement with the weakly coupled grain model fitting described above for all films.

II. Experimental Approach

In order to make a direct measurement of the absorptivity we have used the high-T_c film as the absorbing element in a composite bolometric far infrared detector.[18] The 250 - 500 μm thick substrates are suspended in a thermal vacuum by 100μm thick nylon threads. Typical substrates are 5 $\times$ 5 mm^2. The back surface of each substrate is coated with a gold film to reduce absorption of stray radiation and a small neutron transmutation doped (NTD) germanium thermistor [19] and NiCr heater [20] are glued to this surface. The ~100 ms thermal time constant $\tau = C/G$ of the bolometer is determined by the heat capacity C of the assembled bolometer and the thermal conductance G due to the electrical leads from the thermistor to the heat sink at 2K.

A schematic of the experimental apparatus is shown in Fig. 1. Infrared radiation (A) chopped at 10 Hz from a Fourier transform spectrometer operated in the step-and-integrate mode passes through a light pipe and a cold low pass filter to a roof mirror (B) which divides the beam symmetrically between the sample bolometer (I) and a reference bolometer with known absorptivity (II). The aperture (C) of a thin walled brass tube (not shown) which is pressed against the absorbing film defines the throughput $A\Omega \approx 0.03$ sr-cm^2 onto each film. The absorbing film is located on the front surface of the substrate (E) which is held firmly against the exit of the throughput limiter by tension in the nylon threads (F), which are suspended from a support ring (G). The absorbing films are electrically isolated from the throughput limiters and are surrounded by infrared absorber[21] (D) to reduce stray radiation. The support ring (G) also serves as a heat sink (L) for the electrical connections (H) to the thermistor (J) and heater resistor (K). Frequency dependent asymmetries in the throughput are measured and corrected by interchanging sample and reference detectors.

The frequency dependence of the response to an ac current through the heater and to chopped infrared radiation are measured to confirm that all internal thermal relaxation times in the bolometer are much shorter than C/G. Under these conditions the responsivity R^f of the bolometer to absorbed infrared power at frequency f can be measured by passing an ac current at frequency $f/2$ through the known heater resistance.

The output spectrum from each detector channel can be represented by $F(v) = L(v) A(v) R^f$ where v is the wavenumber (cm⁻¹), $L(v)$ is the submillimeter spectrum incident on the absorbing film from the spectrometer, $A(v)$ is the absorptivity of the film, and R^f is the responsivity of the detector to absorbed power. If the detector responsivities and the absorptivity of the reference detector are known then the absorptivity of the sample can be determined from

$$A_s(v) = \frac{F_s(v) \, R_r^f}{F_r(v) \, R_s^f} \, A_r(v) \, , \tag{1}$$

where the subscripts s and r refer to the sample and reference channels, respectively, and where $A_r(v)$ is the known absorptivity of the reference absorber.

The success of this experiment depends on the availability of a reference film with known absorptivity. In addition, the reference absorber should have a small heat capacity and an absorptivity comparable to that of the sample. For this reason we use a sputtered gold film. No special precautions are taken to insure the purity of the sputtered metal and so the conductivity of the film is low enough that the absorptivity can be calculated from the classical skin effect theory using the conductivity $\sigma(\omega) = \sigma_{dc} / (1 - i\omega\tau)$. Here $\sigma_{dc} = ne^2\tau/m$ is the dc conductivity of the gold film measured at 4K and τ is the momentum relaxation time inferred from σ_{dc} assuming a free electron mass and a carrier density of one electron per atom.[22]

Because of surface imperfections the optical absorptivity calculated from the bulk dc properties will underestimate the actual film absorptivity.[23] In order to correct for this effect we have measured the absorptivity of an etched brass foil relative to the gold reference. By fitting the ratio of absorptivities of brass and gold to a Drude model for each of the materials we are able to determine an effective dc conductivity and carrier density for both the brass and the gold. The use of these effective parameters should then partially compensate for the effects of surface imperfections.

The absorptivity of the brass is calculated from the classical skin effect theory using the dc conductivity of the brass measured at 4K and the carrier density estimated from a room temperature Hall coefficient measurement [24] assuming a single carrier band. We calculate the ratio of the absorptivities of brass and gold from the respective dc material properties and also from a best fit to the measured infrared ratio. The measured infrared ratio and the absorptivity ratio determined from the dc properties of the brass and gold, as well as the best fit absorptivity ratio, are shown in Fig. 2 . A list of the dc and best fit parameters for the brass and the gold is given in Table I.

The agreement between the directly measured ratio and the ratio determined from the dc properties is quite good between 30 and 650 cm^{-1}; the agreement between the directly measured ratio and the best fit is excellent over the same frequency range. Because the optical data accounts more accurately for the actual surface properties of the gold film than the simple theory, we use the absorptivity of the gold film determined from the best fit of the optical data to characterize the gold film. The correction to the frequency dependent absorptivity of the gold film varies smoothly with frequency. At 30 (700) cm^{-1} the best fit absorptivity is 3%

higher (15% lower) than the absorptivity determined from the dc properties of the gold alone.

Deviations between the best fit and the absorptivity ratio in Fig. 2 help to establish the valid range of the optical data. The reproducibility of the data is poor above 650 cm^{-1}. This may reflect the sensitivity of the spectrometer to thermal drifts at these high frequencies. Deviations are seen below 30 cm^{-1} which appear to be due to the decreasing effectiveness of the light baffles surrounding the sample. The light baffles become transparent below ~30 cm^{-1}.[25] This effect leads to an overestimation of $A(\omega)$. Because the sample and reference absorptivities are not identical this error does not cancel out when the ratio of absorptivities is calculated.

As a test of the method we have measured the absorptivity of a 250 nm Nb film at 2K which is shown in Fig. 3. Note that we are able to observe a superconducting gap in the Nb at ~ 25 cm^{-1} where the absorptivity is less than 0.5%.

III. Sample Characterization

The samples used in this study were fabricated by three different research groups using two different techniques, and were grown on MgO,[26] LaAlO3 ,[27,28] and SrTiO3 [28,29] substrates. A list of the samples studied is found in Table II. Samples A,B,C and E were fabricated with a 90° off - axis sputtering technique from a composite YBCO target.[26,27] Substrates were attached to a substrate block heated to approximately 700° C with either a mechanical clamp or silver paste or both. Approximately 100 Watts of power on the sputter gun gave a deposition rate for the off-axis geometry of less than 0.1 Å/sec, depending on the sputtering atmosphere, which varied between 10 - 100 mTorr O_2 (or N_2O) and 40 - 300 mTorr Ar. Samples D and F were fabricated with a laser deposition technique using a

248 nm KrF excimer laser fired at 1 Hz onto a rotating composite YBCO target.[28,29] The plume of ejected materials was collected onto substrates which were heated to approximately 700° C, with typical deposition rates of 1 Å/sec. A jet of oxygen was directed toward the center of the plume while the background pressure was maintained at approximately 10mTorr.

The samples used in this study are notable for their lack of impurity phase and high degree of epitaxial alignment perpendicular to their surface, with the YBCO c-axis perpendicular to the substrate surface. Compositional analysis with Rutherford backscattering spectrometry indicated that the films used in this study were in the 1:2:3 phase.[27,30,31] Crystalline quality was studied by measuring x-ray rocking curve widths for films nominally identical to those used in this study [26,29,30,32,33] and suggest within the limitations of the experiment that these films have nearly perfect single crystalline structure. However, transmission and scanning electron microscopy studies indicate that these films are heavily faulted. This apparent contradiction between x-ray and electron studies can be resolved by recalling that x-rays are less sensitive to small scale structure than electrons, which have shorter wavelengths and coherence lengths.[29]

The microstructure of the laser deposited films on $LaAlO_3$ and $SrTiO_3$ exhibit undulations both along the (001) planes (c-layers) and the (110) planes, with a typical structural correlation range of about 10 nm.[29] These films are nevertheless free from macroscopic grain boundaries [1,29,30] and are very homogeneous, with surface roughness less than 15 nm, and are free from any secondary phase. In contrast, laser deposited films on MgO, or films deposited onto $LaAlO_3$ or $SrTiO_3$ substrates heated above 700° C, contain grain boundaries of a few μm or larger.[29,34] Typical c-axis oriented films deposited by off-axis sputtering exhibit a high density of intersecting (110) twins, with typical spacings ranging from 10 - 70 nm and with

twin lengths from 20 - 200 nm.[31] Typical surface roughness for c-axis films deposited onto MgO is less than 5 nm.[31] Films deposited on LaAlO$_3$ can be rougher.[33] In addition, the off-axis sputtered films contain a small volume fraction of a-axis oriented grains,[31,33] typically less than 1%.

In plane film texture was examined by studying x-ray ϕ scans.[35] Both LaAlO$_3$, SrTiO$_3$ and the 1:2:3 phase of YBCO have a perovskite structure and the lattice match between these materials is good. However, a 7-9% lattice mismatch for MgO and YBCO in the (001) crystallographic direction may, under non-optimal growth conditions, lead to the formation of grains in which the in plane unit cell axis of the film is aligned with the (110) axis of the substrate, corresponding to a rotation of 45°. The size of these 45° rotated domains ranges from 0.5 to 10.0 μm.[31] Off-axis sputtered films on MgO typically contain less than 1% volume fraction of such misoriented grains and misorientations of other distinct angles.[31]

A positive correlation has been found by others between the volume fraction of high angle (45°) grain boundaries and R$_s$ for YBCO films on MgO.[32] However, other studies of YBCO thin films on LaAlO$_3$ have found a lack of correlation between R$_s$ and structural properties such as the quantity of 45° misoriented material. In fact film E on LaAlO$_3$, with a fairly large R$_s$ = 180$\mu\Omega$, was found to have a very small (.06%) volume fraction of 45° misoriented material.[27]

IV. Microwave Measurements

The microwave surface resistance R$_s$ of samples A, B, C and E was measured at 11 - 13 GHz with a parallel plate resonator technique, described elsewhere.[36] Two flat superconducting films of the same nominal area with a thin dielectric spacer between them form the resonator. By using a dielectric spacer with a small loss tangent and making the spacer as thin as possible it is found that the Q of the

resonator is dominated by the loss in the superconducting film and is therefore inversely proportional to the surface resistance of the film. In this analysis it is assumed that the films are thick enough that rf power is not transmitted through the film. If the films are too thin then the measured value of the surface resistance will be lower than for a thick film of similar material. Values of R_s quoted for the films measured with this technique do not include any correction for radiation loss.[27,32,33,36] The effects of the finite film thickness on these measurements is discussed below.

The surface resistance of sample D was measured by placing it in a superconducting niobium cavity operated in the TE_{011} mode at 5.95 GHz as described elsewhere.[37] The value of cavity Q was converted into surface resistance by comparison with the measured Q and the calculated surface resistance of a Nb foil with nominally the same area as the sample. In this measurement rf currents are induced in both the upper and lower surfaces of the film. The substrate losses are subtracted from the result through a separate measurement of a bare substrate. The resulting value of R_s is an average for the two surfaces and may contain contributions from losses at the interface between the film and the substrate.

The effect of the finite film thickness on the measurement of the microwave surface resistance has been examined by Klein et al. [38] at 87 GHz and 77 K by treating the film - substrate system as a transmission line and approximating the surface impedance of a hypothetical thick slab of superconductor as $Z_\infty = R_\infty - i\, 4\pi\omega\lambda/c^2$, where R_∞ and Z_∞ correspond to the surface resistance and complex impedance, respectively, of the hypothetical thick slab. This treatment is a useful guide to the effects of the finite film thickness on observed surface impedance. The concept of a bulk impedance Z_∞ is of limited validity for high T_c films, however,

since the microstructure of these materials, and hence Z_∞, can depend in a complicated way on sample thickness.[31,36]

   We have done similar calculations at 10 GHz and 4 K using $\lambda = 140$ nm and treating the sample as a thin superconducting film of bulk impedance Z_∞ on a 500 μm substrate of LaAlO$_3$ backed by free space. We find that measured surface impedances at 10 GHz and 4K can depend on film thickness for films thinner than ~500 nm. For films thicker than 300 nm, however, we find that R_∞ will be at most 25% lower than the measured R_s for films with measured $R_s > 10\mu\Omega$. We have done similar calculations at 1 THz, corresponding to the lowest frequencies of the submillimeter absorptivity measurement, and find that no correction to the measured absorptivity is required for the range of measured absorptivities and film thicknesses studied.

V. Results

   Absorptivity data for sample F are plotted in Fig. 4 along with $1 - R(v)$, where $R(v)$ is the reflectivity reported earlier on the same sample.[1] Certain features, such as the small knee just below 500 cm^{-1} and the plateau between 200 and 400 cm^{-1} exist in both data sets, but there are differences in the overall level and slope. The two data sets can be brought into very good agreement if we plot $0.85(1 - R(v)) +$ 1.1%. The additive constant may reflect the uncertainty associated with knowing the precise signal level corresponding to unity reflectivity in the reflectivity measurement. The reason for the discrepancy in slope is not known.

   In order to test whether the discrepancy in Fig. 4 could be due to the loss of oxygen from the film in the three months between the reflectivity measurement and the absorptivity measurement, the absorptivities of this and several other films were measured before and after plasma oxygenation and ion bombardment.

Ratios of spectra measured before and after treatment showed observable differences which were fractionally more important in the low frequency part of our range, but neither the sign of the effect nor the frequency dependence were reproducible.

Absorptivity data for samples A through E are plotted in Fig. 5. The absorptivities for all samples are non-vanishing down to the lowest frequencies measured. Despite the varying deposition techniques and substrates, the infrared absorptivity spectra for samples A through D are qualitatively similar. (Sample E was intentionally sputtered in an O_2 deficient atmosphere in order to have higher loss than the other films.) This indicates that although we may not be observing the intrinsic absorptivity of the YBCO we are at least observing a reproducible optical signature which is insensitive to the detailed sample characteristics of high quality films. For these films the absorptivity is roughly monotonic. It increases from the lowest frequencies up to 300 cm^{-1} and has a plateau from ~300 - 450 cm^{-1} above which there is an onset of additional absorptivity. There is no sign of any gap-like onset of absorption near the BCS value of 3.5 $k_BT_c \approx$ 220 cm^{-1} nor is there any indication that the absorptivity is zero below ~ 140 cm^{-1}.[1-3,6,7] We observe distinct optical features in sample E at 150 cm^{-1} and at 310 cm^{-1} which are weakly present in sample A at 150 cm^{-1} and in all films measured at 310 cm^{-1}. These features have been identified as infrared active lattice modes.[39]

Because of the low critical field H_{c1} for the ceramic superconductors it is certain that there is trapped flux in thin films at low temperatures due to the laboratory magnetic field. Flux motion driven by the incident radiation is a potential source of the loss in these films. In order to explore this effect, fields of approximately 10 Gauss were applied normal to the films with both the smallest

and largest microwave R_s. No significant differences in the measured absorptivities were observed.

VI. Data Analysis

A. Introduction

Absorptivity data for samples A through E are again plotted in Fig. 6 along with two theoretical fits described below. This logarithmic plot emphasizes the low frequency range of the submillimeter measurement and allows a comparison with the microwave measurements made on the same samples. The curves in this plot are displaced by factors of ten to avoid overlap. The microwave loss measurements at 4K are indicated by the filled circles for each film. The size of the circles is large enough to include estimated errors and corrections for film transparency. The solid lines give the submillimeter absorptivity measurements at 2K. Additive errors are thought to be small down to the lowest frequencies presented. Multiplicative errors could be as large as 15 percent (see Sec. II). These results give a picture of the residual loss in epitaxial a-b plane YBCO films over nearly four decades in frequency. For each film, the 10 GHz point can be connected to the submillimeter data at ~ 30 cm^{-1} by a line which varies as frequency squared. This agrees with Piel et al.[14] in the range from 10 to ~100 GHz (0.3-30 cm^{-1}), but is in disagreement with Renk et al.[5] who observe the loss to be linear in frequency between 87 GHz (~ 3 cm^{-1}) and 30 cm^{-1}. The frequency dependence of the loss saturates smoothly above 30 cm^{-1} in a way that is different for different films. In contrast to the results of Pham et al.[16] on single crystals we do not observe the loss to vary quadratically with frequency in the range from 100 to 400 cm^{-1}.

We have analyzed data for films A through E in terms of a simple two-fluid model and in terms of a model proposed by Hylton et al. [40,41] that treats

polycrystalline high T_c films as a network of weakly coupled grains. We have also used the KK transform method to calculate the complex conductivity $\sigma(\omega)$ from the loss data for each sample.

B. Two-Fluid Model

The two-fluid model is often used to describe the electrodynamics of a homogeneous, isotropic superconductor below the gap frequency.[42] Some temperature dependent fraction n_s/n of the electrons is in the condensed phase, or superconducting state while the remainder n_n/n are in the excited, or normal state. In the implementation of the two-fluid model used here, the fraction of normal electrons n_n/n is assumed not to have the usual temperature dependence but is used as a free parameter. The conductivity can be written as

$$\sigma(\omega) = \frac{\sigma_0}{1 - i\,\omega\tau} + i\frac{c^2}{4\pi\lambda_{tf}^2\omega} \qquad (2)$$

The complex normal (quasiparticle) conductivity is written in terms of $\sigma_0 = \sigma_{dc}(n_n/n)$ where $\sigma_{dc} = ne^2\tau/m$ is the normal state conductivity and τ is the momentum relaxation time. The complex superconducting (pair) conductivity is given in terms of the superconducting penetration depth, λ_{tf}, where

$$\frac{1}{\lambda_{tf}^2} = \frac{4\pi}{c^2}\frac{n_s e^2}{m} \quad .$$

Here m and e are the mass and charge, respectively, of the paired carriers.

We can describe the two-fluid model in terms of an equivalent circuit with frequency independent lumped circuit elements, as shown in Fig. 7(a). The normal carrier inductivity is $\mathcal{L}_n = m/n_n e^2 = \tau/\sigma_0$ and the superconducting carrier inductivity is $\mathcal{L}_s = m/n_s e^2 = 4\pi\lambda_{tf}^2/c^2$. The inductance per square of a film is equal

to the inductivity divided by the film thickness. The free parameters for this model are λ_{tf}, σ_0 and τ.

At low frequencies for which $\mathcal{L}_n, \mathcal{L}_s \ll 1/\omega\sigma_0$, the penetration of the rf fields is limited by the superconducting electrons, and the absorptivity $A(\omega) = \beta_l \omega^2$ where $\beta_l = \sigma_0 \mathcal{L}_s^{3/2}/\pi^{1/2} = 8\pi\sigma_0\lambda_{tf}^3/c^3$. At intermediate frequencies for which $\mathcal{L}_s \gg 1/\omega\sigma_0 \gg \mathcal{L}_n$, the penetration is limited by the normal electrons and the absorptivity $A(\omega) \propto \omega^{1/2}$. Above the relaxation frequency of the normal electrons $\mathcal{L}_n, \mathcal{L}_s \gg 1/\omega\sigma_0$ and the absorptivity $A(\omega) = \beta_h$ where $\beta_h = \mathcal{L}_s^{3/2}/\sigma_0\pi^{1/2}(\mathcal{L}_s + \mathcal{L}_n)^{3/2}$ is a constant up to the plasma frequency which is outside of our range. For non-vanishing $\tau = \sigma_0\mathcal{L}_n$, however, the intermediate frequency limit is accessible only for $n_n > n_s$. Our data do not show a distinct region in which the absorptivity varies as $\omega^{1/2}$.

C. Weakly Coupled Grain Model

Hylton et al. [40] proposed a model that treats polycrystalline high T_c films as a network of weakly coupled grains, as suggested by the morphology of high T_c superconducting films. In c-axis oriented YBCO thin films the current flows in the strongly superconducting a-b planes, but is impeded by grain boundaries.[43] Hylton et al. proposed a phenomenological model that ignores the anisotropy of the electrical conductivity in the a-b plane and assumes that the material of the grains is an ideal BCS superconductor. The grain boundaries are modeled by resistively shunted Josephson junctions. The distributions of grain size and coupling strength between the grains are then reduced to an effective grain size and coupling strength. It is assumed that the rf current density through the junction is small compared with the critical current I_c of the junction so that the Josephson junction

can be approximated as an inductor $L_j = \hbar/2eI_c$. Introducing a characteristic length associated with the average grain size a the conductivity can be written as

$$\sigma(\omega)^{-1} = -i\omega \mathcal{L}_g + \left[\frac{1}{\rho_j} + \frac{1}{-i\omega\mathcal{L}_j}\right]^{-1} , \qquad (3)$$

where the superconducting inductivity of the grains is $\mathcal{L}_g = 4\pi \lambda_g^2/c^2$, the inductivity of the Josephson junction is $\mathcal{L}_j = \hbar/2ej_c a = 4\pi \lambda_j^2/c^2$. We obtain a shunt resistivity ρ_j for the junctions by assuming that the grains have characteristic length a. The parameter j_c is the critical current density of the grain boundary junction, λ_g is the penetration depth within the grains, and λ_j is the Josephson penetration depth of the junction. The equivalent circuit that represents this response is shown in Fig. 7(b). The effective superconducting penetration depth λ_{eff} that would be measured in a magnetic field penetration experiment[41] is given by

$$\lambda_{eff}^2 = \lambda_g^2 + \lambda_j^2 . \qquad (4)$$

This parameter includes the effects of both the superconducting grains and the Josephson coupling between the grains.

The functional form for $\sigma(\omega)$ in the two-fluid model is identical to that in the weakly coupled grain model. Expressing the parameters of the two-fluid model in terms of the weakly coupled grain model parameters, we find

$$\mathcal{L}_s = \mathcal{L}_g + \mathcal{L}_j \qquad (5a)$$

$$\mathcal{L}_n = \left(\frac{\mathcal{L}_g}{\mathcal{L}_j}\right)\left(\mathcal{L}_g + \mathcal{L}_j\right) \qquad (5b)$$

$$\sigma_0^{-1} = \rho_j \left(\frac{\mathcal{L}_g + \mathcal{L}_j}{\mathcal{L}_j}\right)^2 \qquad (5c)$$

Eq. 5a is equivalent to Eq. 4 and shows that λ_{tf} in the two-fluid model is equal to λ_{eff} in the weakly coupled grain model.

D. Model Fitting

The two phenomenological models described above yield a single, three parameter frequency dependent conductivity $\sigma(\omega)$. The parameters can be interpreted either in terms of the two-fluid or in terms of the weakly coupled grain model. The three parameter conductivity $\sigma(\omega)$ is used to calculate the absorptivity $A(\omega)$, from

$$A(\omega) = 1 - \left| \frac{\frac{4\pi}{c} - Z(\omega)}{\frac{4\pi}{c} + Z(\omega)} \right|^2 \quad , \tag{6}$$

where $Z(\omega) = (4\pi/c)(\varepsilon_\infty + i\, 4\pi\sigma(\omega)/\omega)^{-1/2}$, and where the film is assumed to be much thicker than the penetration depth. The value of ε_∞ includes the effects of absorption above ~ 1000 cm^{-1}. We find that for $\varepsilon_\infty < 20$ the precise value of ε_∞ has no effect on the data analysis below ~700 cm^{-1}. As a consequence, the fitting function $A(\omega)$ contains just three independent parameters.

The three parameter fitting function was fit to the absorptivity spectra by a chi-squared minimization. A subset of twenty submillimeter points along with the microwave data point were used in the fitting for each sample. The data from the submillimeter spectral range were chosen to lie between ~40 - 400 cm^{-1} to avoid the onset of additional absorptivity above 450 cm^{-1} and were uniformly spaced in Log[frequency] so as not to overemphasize higher frequency data. When features such as the optical phonon at 150 cm^{-1} are avoided the absorptivity spectra are smooth and the precise values of the chosen frequencies are unimportant. The statistical uncertainty used in fitting the data was arbitrarily set equal to 15% of the

loss measured at each frequency. The three parameter fitting function can be made to agree quite well with the data. However, since the data below the absorption edge at 450 cm^{-1} do not contain enough information to uniquely determine all three independent parameters, fits can be obtained for a range of parameter values. Consequently, we use the penetration depth of 140 nm obtained from μsr experiments[44] to constrain the models.

The most natural way to constrain the two-fluid model with the μsr result is to set λ_{tf} = 140 nm. (This is exactly the same constraint as setting λ_{eff} = 140 nm in the weakly coupled grain model.) Results of the fitting with $\lambda_{tf} = \lambda_{eff}$ = 140 nm for samples A through E are shown in Fig. 6 as the short-dashed lines. A good fit to the measured absorptivity is found for samples A, B and D which smoothly joins the submillimeter data to the microwave R_s. However, this fitting function is unable to fit the data for samples C and E. In the case of film E, which has high residual loss, the fit does not even intersect the data. The fit can be forced to intersect the data, but the resulting slope at high frequencies is then so small that the value of chi-squared is increased. Results of this analysis are shown in Table III. Uncertainties for each sample in Table III are estimated from constant chi-squared boundaries which define an arbitrary confidence region about the best fit. Errors indicate relative uncertainties between the parameters and do not include any uncertainty in λ_{eff}.

Alternatively we can use the μsr data to constrain the weakly coupled grain model. This goal is complicated by the interpretation of the μsr data for inhomogeneous materials. The magnetic distribution within the bulk of the material, i.e., the grains, can be approximated by a perfect vortex lattice. Defects at inhomogeneities such as grain and twin boundaries, however, tend to pin the magnetic vortices which then increase the field variation.[45] In principle, the μsr

experiment measures the volume-weighted distribution of magnetic fields throughout the sample. In practice, there is a tendency to focus on the rather narrow distribution of fields in the grains which comprise most of the sample volume rather than the broader distribution of fields in the grain or twin boundaries which comprise a much smaller volume. To the extent that this is the case, the μsr experiment measures λ_g, and not λ_{eff}.

The fits to the weakly coupled grain model, constrained by the μsr measurement[44] with $\lambda_g = 140$ nm, are shown in Fig. 6 as the long-dashed lines. Good fits are obtained to the submillimeter data and the microwave R_s for all five films measured. Results of this analysis are listed in Tables IV and V. In addition, the weakly coupled grain model with $\lambda_g = 140$ nm is in excellent agreement with results from a KK analysis, described in Section VI G. These results suggest that the losses in epitaxial a-b plane films of YBCO are consistent with the weakly coupled grain model when $\lambda_g = 140$ nm. In the following section we therefore focus on the best fits with $\lambda_g = 140$ nm.

E. Discussion of the best fits with $\lambda_g = 140$ nm

Any analysis of submillimeter data using the weakly coupled grain model suffers from the problem that most of the discussions in the literature use two-fluid concepts which are only appropriate for a homogeneous material. In order to make contact with this literature we convert the weakly coupled grain model parameters obtained by setting $\lambda_g = 140$ nm to the two-fluid model parameters σ_0, $\hbar/\tau$ and $\lambda_{tf} = \lambda_{eff}$ which give the same excellent fit to the absorptivity. The values of the two-fluid and weakly coupled grain parameters obtained in this way are also listed in Tables IV and V. The reader is reminded that the two-fluid model does not fit the absorptivity data when λ_{tf} is constrained to the value measured by μsr.

However, the two-fluid model does give good fits to the absorptivity data for a range of other values of λ_{tf}, including the particular values of $\lambda_{tf} = \lambda_{eff}$ listed in Tables IV and V. In spite of these difficulties it is useful to use two-fluid language in addition to weakly coupled grain language to discuss the results of the fitting with $\lambda_g = 140$ nm.

Reflectivity measurements made on YBCO thin films at temperatures just above $T_c \sim 90K$ obtain values of $\hbar/\tau \sim 100$ cm^{-1}. Assuming a BCS gap of 3.5 $k_B T_c$ this result implies that YBCO is in the clean limit of the classical skin effect regime of superconductivity ($\hbar/\tau << 2\Delta$; $\xi_0 << l << \lambda_L$).[1] It is reasonable to assume that the scattering rate $\hbar/\tau$ should decrease with decreasing temperature.[1] However, at low temperature we find scattering rates of 150 cm^{-1} > $\hbar/\tau$ > 700 cm^{-1} for all films measured, corresponding to values of the electronic mean free path l between 2 and 7 nm, assuming $v_F = 2.2 \times 10^7$ cm s^{-1}.[11] It is interesting to speculate on possible explanations for a faster scattering at low temperatures, which is a property of both the parameters of Table III and of Tables IV and V.

A scattering rate $\hbar/\tau$ which is larger in the superconducting state than above T_c can be understood if we postulate that the film contains two types of carriers, which we call "good electrons" and "bad electrons". The "good electrons" condense rapidly into the superconducting ground state below T_c as in a BCS superconductor. The "bad electrons" remain in the normal state at all temperatures. If the "good electrons" have a slow scattering rate and a large oscillator strength and the "bad electrons" have a fast scattering rate and a relatively small oscillator strength then the effective conductivity of the composite system above T_c will be dominated by the "good electrons." Below T_c where the "good electrons" have all condensed the scattering will be dominated by the "bad electrons" and a faster scattering rate will be measured.

Values of λ_{eff} calculated from the parameters in Table IV and given in Table V range from 200 to 520 nm and are consistent with the results from microstrip resonator measurements.[46] As expected, values of λ_{eff} in Table V are larger than penetration depths determined from μsr measurements.[44] This is consistent with our interpretation of μsr experiments, which we have argued measure the penetration depth within the grains, λ_g, and not in the bulk, so that $\lambda_{eff} > \lambda_g$.

The superconducting penetration depth can also be found from infrared measurements by determining the 'missing area' between $\sigma_1(\omega) = \text{Re}[\sigma(\omega)]$ in the normal and superconducting states. This 'missing area' is oscillator strength which condenses into a delta function at zero frequency upon entering the superconducting state, and is related to the number of condensed carriers and thus to the superconducting penetration depth.[47] 'Missing area' calculations based on reflectivity measurements using single crystals obtain values for the penetration depth which are consistent with the μsr result of 140 nm,[2,3] not with λ_{eff} as might be expected from the weakly coupled grain model. Differences between the losses in thin films and crystals may account for some of this discrepancy. However, above 400 cm^{-1} the loss in films A, B and D are nearly identical to the losses in YBCO single crystals with $T_c \sim 90$ K.[2,3] Another possible explanation is a difference between the absorptivity assumed in interpreting the two experiments. In the missing area calculations the superconducting state conductivity $\sigma_1(\omega)$ below 140 cm^{-1} was taken to be either zero[2] or constant[3] and equal to $\sim$1400 $(\Omega - \text{cm})^{-1}$. As discussed in Sec. VI G, we find a larger oscillator strength below 140 cm^{-1} both from the weakly coupled grain best fits with $\lambda_g = 140$ nm and from the KK analysis of our loss data. This would tend to increase the value of λ_{eff} determined from missing area arguments, but only inversely as the square root of the area difference. A third possible explanation is that grain models can be expected to fail at high enough

frequencies that the coherence length of the radiation becomes small compared with typical grain sizes.

The fraction of normal state carriers n_n/n determined from the parameters in Table IV range from 0.6 to 1.6 % at 2K, more than four orders of magnitude larger than the prediction of the Gorter-Casimir two-fluid model, where $n_n/n = (T/T_c)^4$. From the parameters in Table III we find values for n_n/n which range from 2 to 13 %. These larger values are closer to the results of Gao et al.[9] who use a two-fluid model to fit their reflectivity data, obtaining values of n_n/n at low temperature between 10 and 50 %.

For the weakly coupled grain model we have determined the $I_c R = \rho_j j_c \, a$ product and the characteristic grain length a of the junction. In order to determine a we must assume a value for the critical current density j_c, since only the product $j_c a$ is determined from the weakly coupled grain model. We assume that the critical current density j_c of the grain boundaries is essentially the critical current density 3×10^7 A cm^{-2} of the films, which is a typical value for high quality c-axis films at 4K,[31] in agreement with measurements made on films A and B.[31,32] $I_c R$ products in Table V are consistent with measurements on isolated grain boundary junctions, which range between 0.2 and 8 mV at 4.2K.[43] Characteristic grain lengths a range from 4 to 40 nm for all films. These values are roughly consistent with the spatial correlation range in the laser ablated films of ~ 10 nm,[29] and with twin domain sizes in off-axis sputtered films of ~ 20-200 nm.[31]

Although the weakly coupled grain model is able to fit our loss data so well, values of a found from the best fits are considerably smaller than the size of typical 45° misoriented grains, which range from 0.5 to 10.0 μm.[31] Such high angle grain boundaries are known to behave as resistively shunted junctions[43] which could therefore justify the use of the weakly coupled grain model. However, the volume

fraction of such grains in our films is typically less than one percent,[31,32] which is an indication that the high angle grain boundary junctions probably do not provide the dominant intergrain coupling mechanism in these films. The parameter values deduced from fitting the weakly coupled grain model, however, are quite reasonable considering the simplicity of the model.

F. Including Oscillator Strength Above 140 cm^{-1}

The technique we have used to fit our data explicitly assumes that the absorption mechanism above 450 cm^{-1} does not contribute any oscillator strength below that frequency. In order to test the sensitivity of the weakly coupled grain and two-fluid model parameters to this assumption, we have analyzed our data including oscillator strength peaked at ~1000 cm^{-1} proposed by other investigators.[1,12] While the addition of this high frequency oscillator strength reduces the oscillator strength at lower frequencies required to fit the data, the effect is quantitatively small and the model parameters obtained in this way are all within the experimental uncertainties reported for the fits with both λ_{eff} = 140 nm (Table III) and λ_g = 140 nm (Tables IV and V).

G. Kramers-Kronig Analysis

As an alternative to the model fitting described above, we have also used the KK transform technique to deduce the frequency dependent conductivity, $\sigma(\omega)$, from our loss data. In contrast to the fitting procedure, the KK technique requires a knowledge of the loss, or equivalently the reflectivity, for all frequencies. In all practical cases the loss is measured over some finite frequency interval and extended to zero and infinite frequencies, respectively, by suitable extrapolations. Care must be taken in extending the loss data as considerable uncertainties in the

inferred conductivity may result, even at frequencies far from the range of the extrapolations.

We extend our absorptivity data to higher frequencies in two different ways. We have smoothly grafted our data, which ends at 700 cm^{-1}, onto reflectivity data for a similar sample[48] which extends to 5 eV. This reflectivity is roughly constant, with R ~ 0.08 near 5 eV. We then extrapolate the data to infinite frequency by assuming that the reflectivity remains constant above 5 eV. We have also grafted our loss data onto the data of Tajima *et al.*,[49] which extends to 35 eV. Above this frequency we have extrapolated the reflectivity measured by Tajima *et al.* by an ω^{-4} dependence, which is the free electron asymptotic limit. Despite the difference between these extrapolations, the conductivities determined by the KK transform for both of these high frequency extrapolations are nearly identical below 2000 cm^{-1}. The contributions to the low frequency conductivity from both high frequency reflectivity extrapolations are consistent. In addition, the conductivity below ~600 cm^{-1} is independent of the precise way in which the sets of measured data are grafted together.

We extend our data to zero frequency by assuming that the loss varies as ω^2 below ~30 cm^{-1}. Within experimental uncertainty this extrapolation intersects the measured microwave loss R_s for all films and is consistent with the results of all of the model fitting described in Sec. VI.

The results of this analysis are shown in Fig. 8 where we plot $\sigma_1(\omega) = \text{Re}[\sigma(\omega)]$ for sample B. The solid line is obtained from the KK transform; the short-dashed line is the best fit of the two-fluid model with $\lambda_{tf} = 140$ nm or of the weakly coupled grain model with $\lambda_{eff} = 140$ nm from Table III; and the long-dashed line is the best fit of the weakly coupled grain model with $\lambda_g = 140$ nm from Table IV. This figure is representative of the results obtained for all samples. We find

remarkable agreement between the conductivity determined from the KK transform and that from the weakly coupled grain model with $\lambda_g = 140$ nm. This agreement supports the weakly coupled grain model as a phenomenological description of the submillimeter and millimeter wave losses in YBCO. In particular, this agreement gives us confidence in our interpretation of λ_g as the superconducting penetration depth which is analogous to the penetration depth measured by μsr techniques, as discussed in Sec. VI C and D. In contrast, the conductivity determined from fits to the two-fluid model with $\lambda_{tf} = 140$ nm or to the the weakly coupled grain model with $\lambda_{eff} = 140$ nm are consistently larger than the results of the KK analysis for frequencies below 700 cm^{-1}.

The results for $\sigma_1(\omega)$ from the KK transform are in agreement with those from other workers, both in magnitude and overall shape for frequencies above ~400 cm^{-1}.[1-6] In particular, we observe the well known conductivity onset at 450 cm^{-1}. Below 400 cm^{-1} we observe that the conductivity rises slowly to a maximum at $\omega = 0$ with values of $\sigma_1(0)$ ranging from 3000 to 8000 $(\Omega$ cm$)^{-1}$ for all samples. This result is consistent with two recent reflectivity experiments,[4,5] one of which was extended with a measurement of the microwave loss at 87 GHz.[5] However, below 400 cm^{-1} our result is in disagreement with the low temperature, low frequency conductivity determined from KK transforms of reflectivity data,[1,2,6] from a combined transmissivity and reflectivity measurement,[9] and from another direct absorptivity measurement on single crystals.[16] Possible sources for this discrepancy will be discussed in a future publication.[50]

VII. Conclusions

We have measured the residual loss in six a-b plane epitaxial thin films of YBa$_2$Cu$_3$O$_7$ from 30 cm^{-1}(1.5 THz) to 700 cm^{-1} (21 THz) and for five of the six films

near 0.3 cm^{-1} (10 GHz). We do not observe any gap-like features below 450 cm^{-1} nor is there any indication that the absorptivity is zero below ~ 140 cm^{-1}. For each of the five films the loss measured near 0.3 cm^{-1} can be connected to the submillimeter data at ~30 cm^{-1} by a line which varies as the frequency squared. Above ~30 cm^{-1} the loss saturates smoothly in a way which is different for different films. Above 450 cm^{-1} there is a sudden onset of additional absorptivity and the loss data diverge rapidly from model fits, suggesting the onset of an additional absorption mechanism.

We have used both a homogeneous two-fluid and an inhomogeneous weakly coupled grain model for the electrical conductivity to fit the frequency dependent absorptivity. Both of these models yield the same three parameter fitting function. We find that the homogeneous two-fluid model is unable to fit the data for all films measured when the parameter corresponding to the superconducting penetration depth λ_{tf} is constrained by the μsr result. However, the inhomogeneous weakly coupled grain model is able to smoothly fit the data from 0.3 cm^{-1} (10 GHz) to 450 cm^{-1} (13.5 THz) when the parameter λ_g corresponding to the superconducting penetration depth within the BCS like grains is constrained by the μsr result. In addition, we find remarkable agreement between the results of a KK analysis and the best fits from the weakly coupled grain model below 450 cm^{-1} for all films. These results suggest that weak link behavior may play a significant role in the microwave and submillimeter losses. Values of junction I_cR products and a characteristic length determined from the model best fits are consistent with these independently measured quantities.

References

1.   K. Kamaras, L.L. Herr, C.D. Porter, N. Tache, D.B. Tanner, S. Etemad, T. Venkatesan, E. Chase, A. Inam, X.D. Wu, M.S. Hegde and B. Dutta, Phys. Rev. Lett. **64**, 84 (1990)

2.   J. Orenstein, G.A. Thomas, A.J. Millis, S.L. Cooper, D.H. Rapkine, T. Timusk, L.F. Schneemeyer and J.V. Waszczak, Phys. Rev. B **42**, 6342 (1990)

3.   Z. Schlesinger, R.T. Collins, F. Holtzberg, C. Field, G. Koren and A. Gupta, Phys. Rev. B **41**, 11237 (1990)

4.   D. vanderMarel, M. Bauer, E.H. Brandt, H.U. Habermeier, D. Heitmann, W. Konig and A. Wittlin, Phys. Rev. B **43**, 8606 (1991)

5.   K.F. Renk, B. Gorshunov, J. Schutzmann, A. Pruckl, B. Brunner, J. Betz, S. Orbach, N. Klein, G. Muller and H. Piel, Europhys. Lett. **15**, 661 (1991)

6.   J. Schutzmann, W. Ose, J. Keller, K.F. Renk, B. Roas, L. Schultz and G. Saemann-Ischenko, Europhys. Lett. **8**, 679 (1989)

7.   G.A. Thomas, J. Orenstein, D.H. Rapkine, M. Capizzi, A.J. Millis, R.N. Bhatt, L.F. Schneemeyer and J.V. Waszczak, Phys. Rev. Lett. **61**, 1313 (1988)

8.   Z. Schlesinger, R.T. Collins, F. Holtzberg, C. Feild, S.H. Blanton, U. Welp, G.W. Crabtree, Y. Fang and J.Z. Liu, Phys. Rev. Lett. **65**, 801 (1990)

9.   F. Gao, G.L. Carr, C.D. Porter, D.B. Tanner, S. Etemad, T. Venkatesan, A. Inam, B. Dutta, X.D. Wu, G.P. Williams and C.J. Hirschmugl, Phys. Rev. B **43**, 10383 (1991)

10.   G.P. Williams, R.C. Budhani, C.J. Hirschmugl, G.L. Carr, S. Perkowitz, B.Lou and T.R. Yang, Phys. Rev. B **41**, 4752 (1990)

11.   B. Batlogg, in <u>High Temperature Superconductivity Proceedings, Los Alamos Symposium 1989</u> , edited by K. S. Bedell, D. Coffey, D. E. Meltzer, D. Pines and J. R. Schrieffer (Addison-Wesley, California, 1990), p. 37

12.   T. Timusk and D.B. Tanner, in <u>Physical Properties of High Temperature Superconductors I</u> , edited by D. M. Ginsberg (World Scientific, New Jersey, 1989), p. 339

13.   T. Timusk, C.D. Porter and D.B. Tanner, Phys. Rev. Lett. **66**, 663 (1991)

14.   H. Piel and G. Muller, IEEE Trans. Magn. **27**, 854 (1991)

15.   D. Miller, T.W. Kenny, P.L. Richards, S.R. Spielman and T.H. Geballe, Bull. Am. Phys. Soc. **34**, 792 (1989)

16.   T. Pham, H.D. Drew, S.H. Moseley and J.Z. Liu, Phys. Rev. B **41**, 11681 (1990)

17.   K.F. Renk, J. Schutzmann, A. Pruckl, B. Roas, L. Schultz and G. Saemann-Ischenko, Physica B **165&166**, 1253 (1990)

18.   N.S. Nishioka, P.L. Richards and D.P. Woody, Appl. Optics **17**, 1562 (1978)

19.   E.E. Haller, Infrared Phys. **25**, 257 (1985)

20.   NiCr resistors are manufactered by Mini-Systems Inc., North Attleboro, Mass. 02761

21.   The infrared absorber is made from precast Eccosorb CR110, Emerson and Cuming, Gardena, CA, USA

22.   C. Kittel, <u>Introduction to Solid State Physics</u> , (Wiley, New York, 1986)

23.   R.G. Chambers and A.B. Pippard, Institute of Metals Monograph **13**, 281 (1953)

24.   W. Koster and H.P. Rave, Z. Metallkde. **55**, 750 (1964)

25.   M. Halpern, H.P. Gush, E. Wichnow and V. deCosmo, Appl. Optics **25**, 565 (1986)

26.   C.B. Eom, J.Z. Sun, K. Yamamoto, A.F. Marshall, K.E. Luther and T.H. Geballe, Appl. Phys. Lett. **55**, 595 (1989)

27.   N. Newman, K. Char, S.M. Garrison, R.W. Barton, R.C. Taber, C.B. Eom, T.H. Geballe and B. Wilkens, Appl. Phys. Lett. **57**, 520 (1990)

28.   A. Inam, M.S. Hegde, X.D. Wu, T. Venkatesan, P. England, P.F. Miceli, E.W. Chase, C.C. Chang, J.M. Tarascon and J.B. Wachtman, Appl. Phys. Lett. **53**, 908 (1988)

29.   D.M. Hwang, T. Venkatesan, C.C. Chang, L. Nazar, X.D. Wu, A. Inam and M.S. Hegde, Appl. Phys. Lett. **54**, 1702 (1989)

30.   A. Inam, X.D. Wu, L. Nazar, M.S. Hegde, C.T. Rogers, T. Venkatesan, R.W. Simon, K. Daly, H. Padamsee, J. Kirchgessner, D. Moffat, D. Rubin, Q.S. Shu, D. Kalokitis, A. Fathy, V. Pendrick, R. Brown, B. Brycki, E. Belohoubek, L. Drabeck, G. Gruner, R. Hammond, F. Gamble, B.M. Lairson and J.C. Bravman, Appl. Phys. Lett. **56**, 1178 (1990)

31.   C.B. Eom, J.Z. Sun, B.M. Lairson, S.K. Streiffer, A.F. Marshall, K. Yamamoto, S.M. Anlage, J.C. Bravman, T.H. Geballe, S.S. Laderman, R.C. Taber and R.D. Jacowitz, Physica C **171**, 354 (1990)

32.   S.S. Laderman, R.C. Taber, R.D. Jacowitz, J.L. Moll, C.B. Eom, T.L. Hylton, A.F. Marshall, T.H. Geballe and M.R. Beasley, Phys. Rev. B **43**, 2922 (1991)

33.   N. Newman, B.F. Cole, S.M. Garrison, K. Char and R.C. Taber, IEEE Trans. Magn. **27**, 1276 (1991)

34.   T.S. Ravi, D.M. Hwang, R. Ramesh, S.W. Chan, L. Nazar, C.Y. Chen, A. Inam and T. Venkatesan, Phys. Rev. B **42**, 10141 (1990)

35.   J. Sizemore, R. Barton, A. Marshall, J.C. Bravman, M. Naito and K. Char, IEEE Trans. Magn. **25**, 2245 (1989)

36.   R.C. Taber, Rev. Sci. Instrum. **61**, 2200 (1990)

37.   H. Padamsee, J. Kirchgessner, D. Moffat, J. Potts, D.L. Rubin, Q.S. Shu, A. Inam, X.D. Wu, L. Nazar, M.S. Hegde and T. Venkatesan, (unpublished)

38.   N. Klein, H. Chaloupka, G. Muller, S. Orbach, H. Piel, B. Roas, L. Schulz, U. Klein and M. Peiniger, J. Appl. Phys. **67**, 6940 (1990)

39.   R. Feile, Physica C **159**, 1 (1989)

40.   T.L. Hylton, A. Kapitulnik, M.R. Beasley, J.P. Carini, L. Drabeck and G. Gruner, Appl. Phys. Lett. **53**, 1343 (1988)

41.   T.L. Hylton and M.R. Beasley, Phys. Rev. B **39**, 9042 (1989)

42.   T. Vanduzer and C.W. Turner, <u>Principles of Superconducting Devices and Circuits</u> , (Elsevier, New York, 1981)

43.   R. Gross, P. Chaudhari, M. Kawasaki and A. Gupta, IEEE Trans. Magn. **27**, 3227 (1991)

44.   D.R. Harshman, L.F. Schneemeyer, J.V. Waszczak, G. Aeppli, R.J. Cava, B. Batlogg, L.W. Rupp, E.J. Ansaldo and D.L. Williams, Phys. Rev. B **39**, 851 (1989)

45.   E.H. Brandt, Phys. Rev. B **37**, 2349 (1988)

46.   S.M. Anlage, H. Sze, H.J. Snortland, S. Tahara, B. Langley, C.B. Eom, M.R. Beasley and R. Taber, Appl. Phys. Lett. **54**, 2710 (1989)

47.   M. Tinkham, <u>Introduction to Superconductivity</u> , (McGraw-Hill, New York, 1975)

48.   K. Kamaras and S. Etemad, Private Communication

49.   S. Tajima, H. Ishii, T. Nakahashi, T. Takagi, S. Uchida, M. Seki, S. Suga, Y. Hidaka, M. Suzuki, T. Murakami, K. Oka and H. Unoki, J. Opt. Soc. Am. B **6**, 475 (1989)

50.   D. Miller and P.L. Richards, (in preparation)

Table I: Parameters used in the Drude model for determining the absorptivities of Au and Brass.

	Carrier density n (10^{22} cm^{-3})		Electrical resistivity ρ ($\mu\Omega$ cm)	
	dc	best fit	dc	best fit
Au	5.9	3.6	5.5	5.9
Brass	19.0	7.4	11.6	11.3

Table II: Samples measured in this work. Values of microwave surface resistance R_s measured at 4K near 10 GHz are scaled to 10 GHz using an ω^2 law, where ω is the microwave frequency.

Sample	Institution	thickness (nm)	Substrate	Tc/δT (K)	Deposition Technique	R_s ($\mu\Omega$)
A	Stanford	500	MgO	85 / 1.0	Off-Axis Sputter	12
B	Stanford	400	MgO	85 / 1.0	Off-Axis Sputter	16
C	Conductus	410	$LaAlO_3$	87 / 1.0	Off-Axis Sputter	30
D	Bellcore	500	$LaAlO_3$	92 / 0.5	Laser Ablation	48
E	Conductus	1250	$LaAlO_3$	87 / 2.0	Off-Axis Sputter	180
F	Bellcore	480	$SrTiO_3$	89 / 0.5	Laser Ablation	...

Table III: Parameters σ_0 and $\hbar/\tau$ of the two-fluid model obtained from a best fit of the absorptivity data for samples A through E with λ_{tf} = 140 nm. The same fit is obtained for the weakly coupled grain model if the constraint λ_{eff} = 140 nm is used. For purposes of comparison, the weakly coupled grain model parameters λ_j and ρ_j obtained in this way are also given.

Sample	σ_0 $\times 10^3 (\Omega \ cm)^{-1}$	$\hbar/\tau$ (cm^{-1})	λ_j (nm)	ρ_j $(\mu\Omega \ cm)$
A	11.7 ± 2.5	566 ± 210	122 ± 9	49 ± 4
B	28.1 ± 7.9	426 ± 215	129 ± 8	26 ± 2
C	26.9 ± 8.7	>280	$139 < \lambda_j \leq 140$	36 ± 2
D	36.2 ± 15.8	305 ± 195	128 ± 11	19 ± 2
E	64.3 ± 62.0	>7000	$118 < \lambda_j \leq 140$	15 ± 14

Table IV: Parameters λ_j and ρ_j of the weakly coupled grain model obtained from a best fit of the absorptivity data for samples A through E with $\lambda_g = 140$ nm. Because the two-fluid model gives the same three parameter fitting function for the absorptivity as the weakly coupled grain model, two-fluid model parameters can be deduced which yield the same fit. The values of σ_0 and $\hbar/\tau$ obtained in this way are also given.

Sample	λ_j (nm)	ρ_j ($\mu\Omega$ cm)	σ_0 $\times 10^3 (\Omega$ cm$)^{-1}$	$\hbar/\tau$ (cm^{-1})
A	148 ± 17	93 ± 25	3.0 ± 0.5	377 ± 80
B	175 ± 30	57 ± 18	6.5 ± 1.5	201 ± 50
C	265 ± 55	216 ± 90	2.8 ± 0.9	596 ± 196
D	160 ± 20	41 ± 9	7.8 ± 1.6	157 ± 31
E	502 ± 100	300 ± 150	2.8 ± 1.0	702 ± 256

Table V: Physical quantities derived from the parameters in Table IV which are obtained by setting λ_g= 140 nm.

Sample	λ_{eff} (nm)	I_cR (mV)	a [a] (nm)	l [b] (nm)	n_n/n [c] (%)
A	204 ± 12	11.0 ± 2.5	40 ± 10	3.1 ± 0.6	0.6 ± 0.1
B	224 ± 23	4.9 ± 1.2	29 ± 12	5.8 ± 1.4	1.3 ± 0.3
C	299 ± 49	8.0 ± 2.1	12 ± 5	2.0 ± 0.6	0.6 ± 0.2
D	212 ± 15	4.2 ± 0.9	34 ± 10	7.4 ± 1.5	1.6 ± 0.3
E	521 ± 96	3.1 ± 0.6	4 ± 1	1.7 ± 0.6	0.6 ± 0.2

[a] Values of the effective grain length, a, are calculated assuming $j_c = 3 \times 10^7$ A cm^{-2}

[b] Values of the electronic mean free path, l, calculated assuming $v_F = 2.2 \times 10^7$ cm s^{-1}

[c] Values for normal state carrier fraction, n_n/n, calculated assuming $\rho_{dc} = 2.0$ $\mu\Omega$ cm

Figure Captions

FIG. 1.   Cross section of the apparatus, which was operated in a thermal vacuum at ~1.5 K. Incident radiation A is split by roof mirror B and sent to detector channels I and II. In each channel a throughput limiter C defines the incident radiation. Stray radiation is absorbed by baffles D. The film being measured is located on the front inner surface of a substrate E which is suspended by nylon threads F from the support ring G. Thermistors J and resistance heaters K are indicated schematically. Electrical connections H to thermistors and resistors provided the thermal conductance between the substrate and the heat sinks L.

FIG. 2.   Ratio of the measured absorptivity of brass and gold, as described in text. The solid line is the experimental data. The dashed line is the best fit of the Drude model to the data. The dash - dot line is the fit of the Drude model using the measured dc properties of the brass and gold.

FIG. 3.   Measured absorptivity of Nb thin film at 2K. The residual resistivity ratio for this film is ~ 6 - 7, and the microwave loss is nominally 20 $\mu\Omega$ at 4K and 10 GHz.

FIG. 4.   Absorptivity of sample F measured directly at 2K by the technique described in this work (dashed line) and deduced from a reflectivity measurement made at Bellcore at 15K (solid line).

FIG. 5.   Measured absorptivity of samples A through E at 2K. Sample E was intentionally prepared to give large microwave loss.

FIG. 6.   Measured submillimeter absorptivities of samples A through E at 2K (solid lines) multiplied by the indicated factors to separate the curves. Also shown are best fits to the two-fluid model (short-dashed lines) and best fits to the weakly coupled grain model (long-dashed lines). Values of the microwave surface resistance measured for each sample at 4K and scaled to 10 GHz are shown as filled circles. Sample E was intentionally prepared to give large microwave loss.

FIG. 7.   Equivalent circuits for (a) two-fluid and (b) weakly coupled grain models. A simple circuit transformation shows that these two circuits yield the same form for the frequency dependent fitting function for the absorptivity. The interpretation of the parameters, however, is different for the two models.

FIG. 8.   Values of $\sigma_1(\omega)$ for sample B determined from a Kramers-Kronig analysis (solid line), from the best fit of either the two-fluid model with $\lambda_{tf} = 140$ nm or the weakly coupled grain model with $\lambda_{eff} = 140$ nm (short-dashed lines) and from the best fit of the weakly coupled grain model with $\lambda_g = 140$ nm (long-dashed lines).
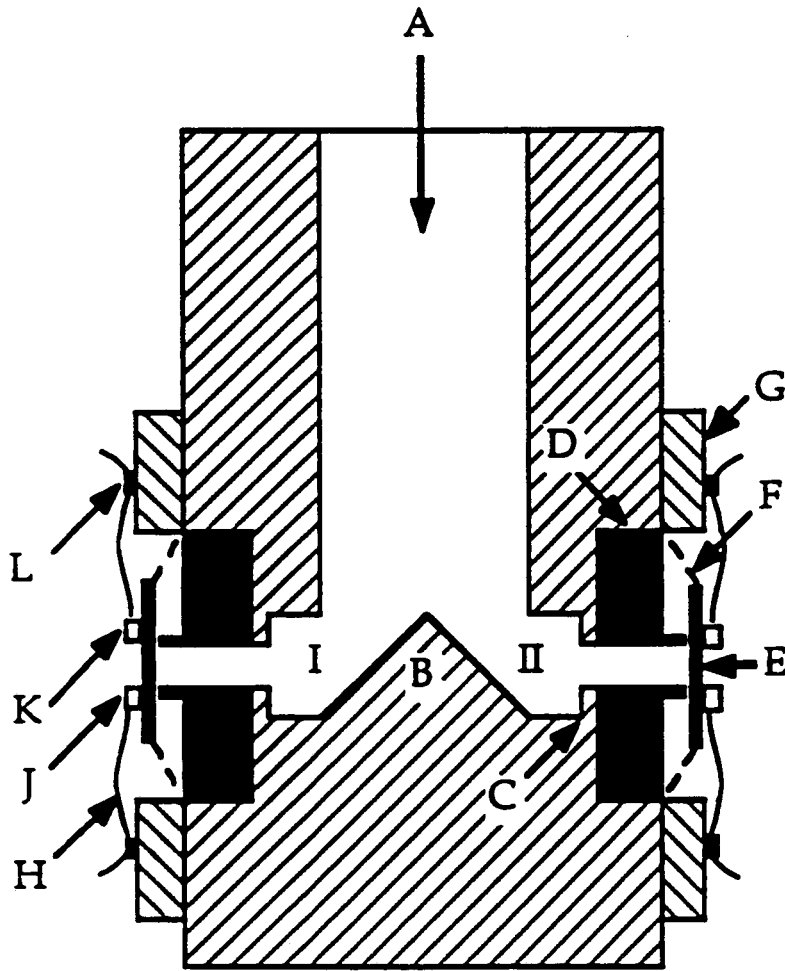
XBL 915-1040
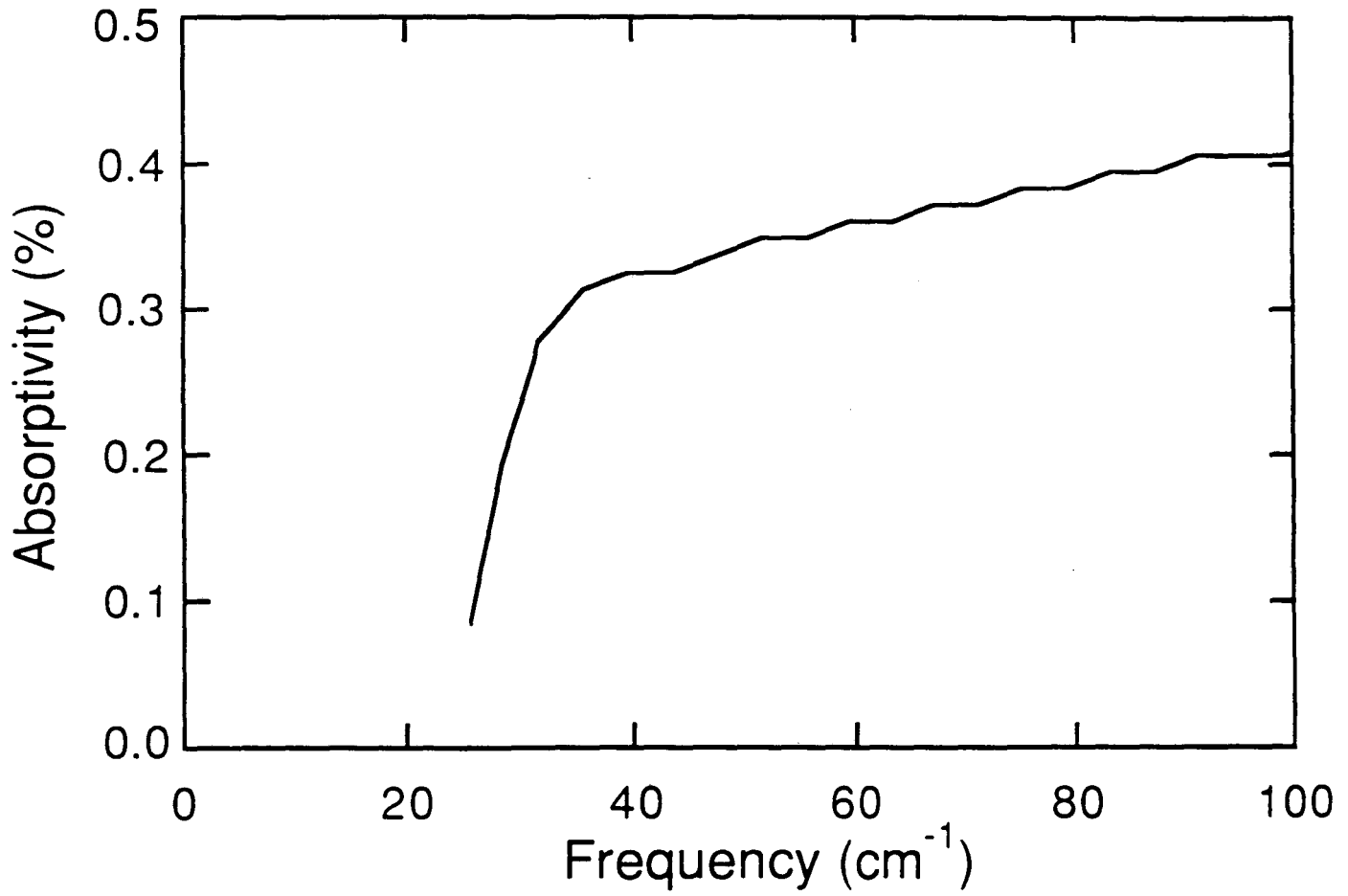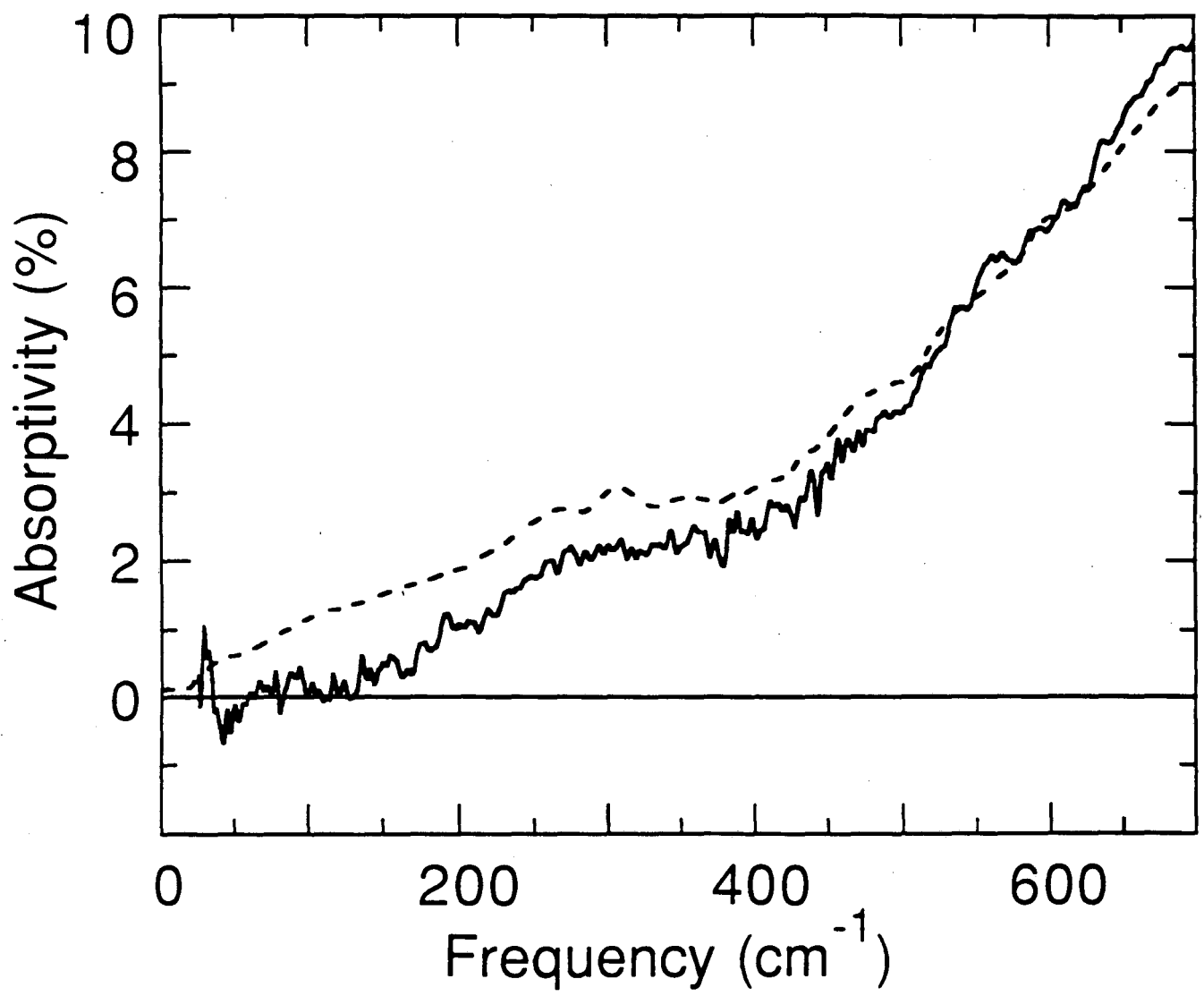
FIGURE 1
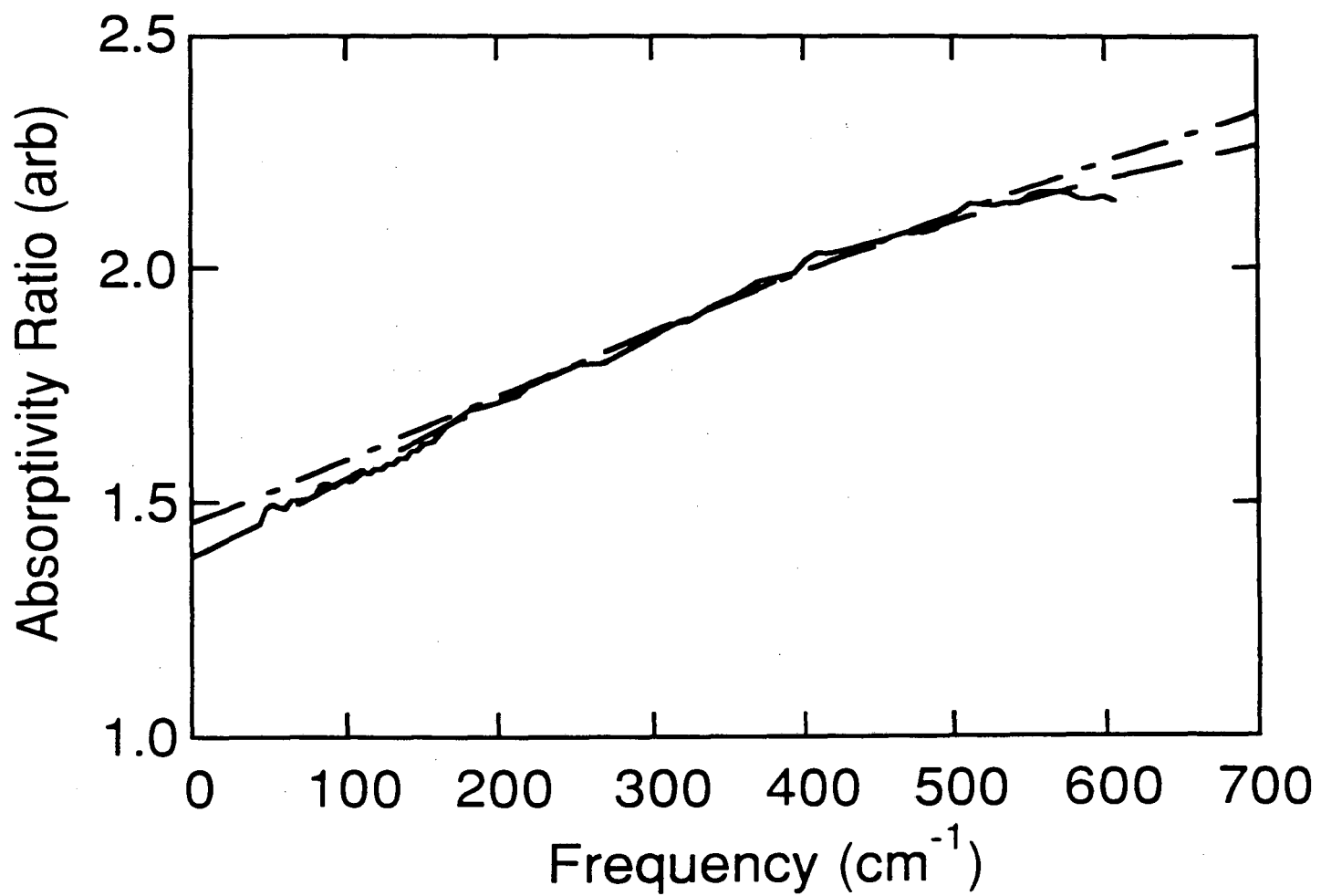
FIGURE 2

FIGURE 3

XBL 919-2016
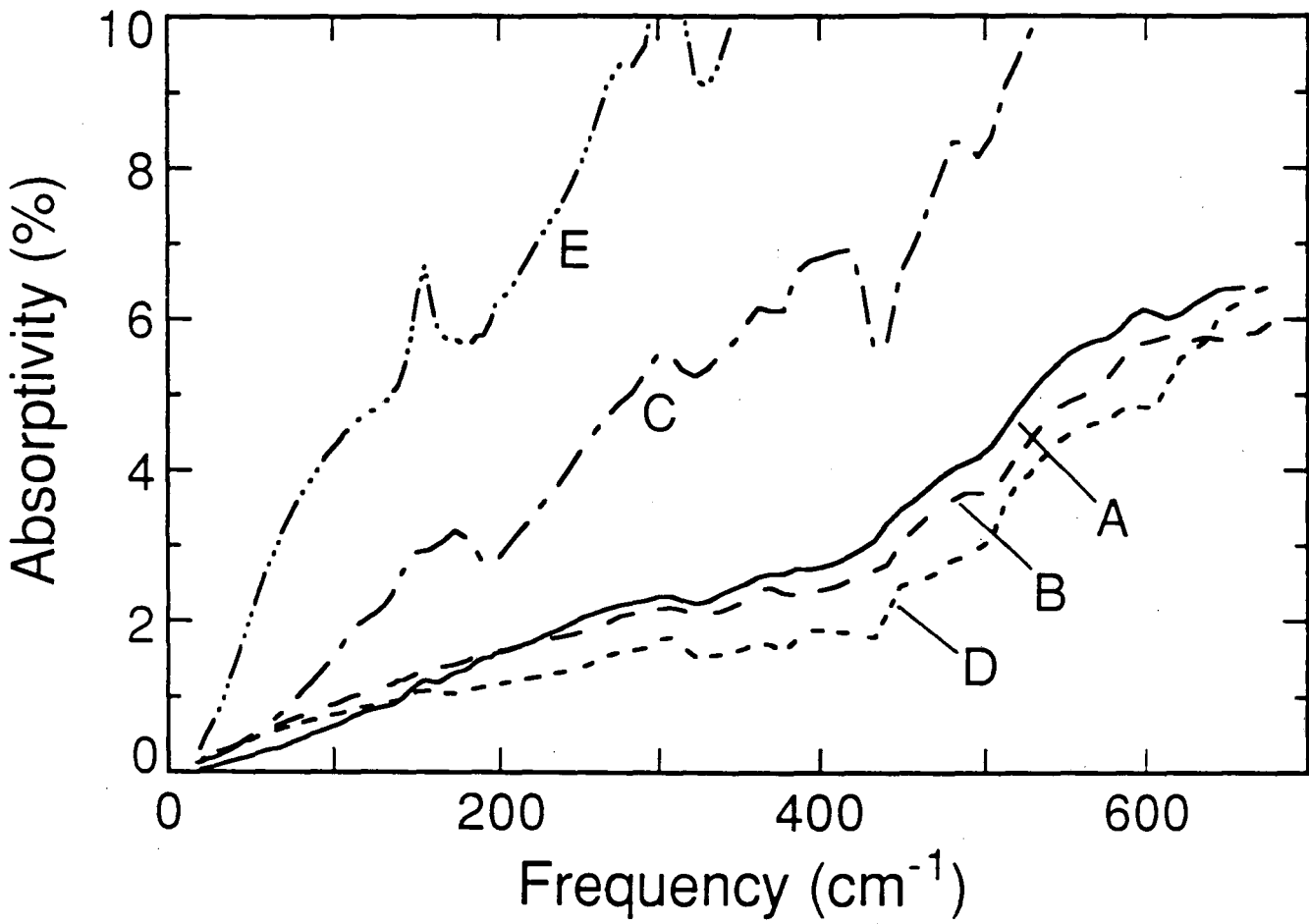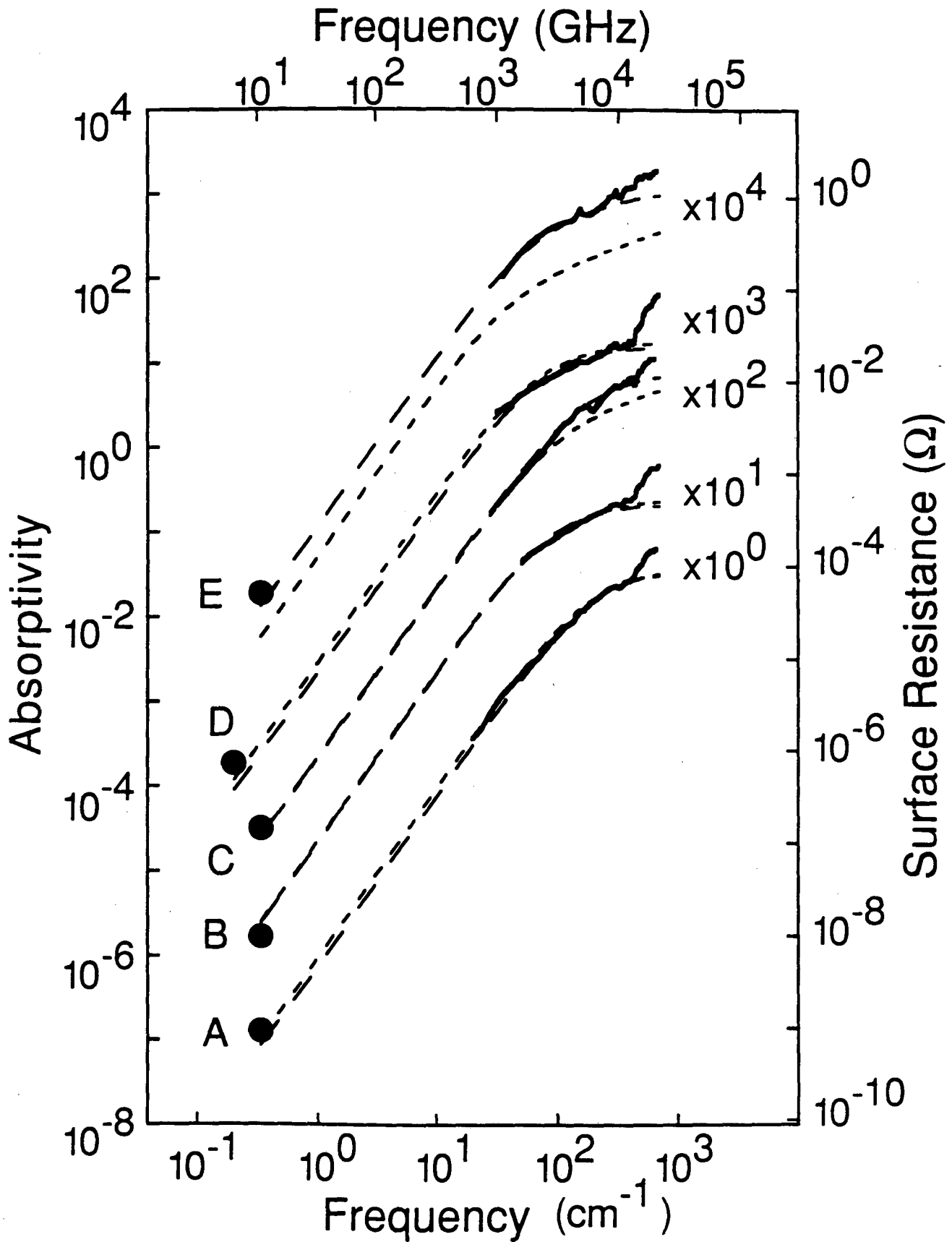
FIGURE 4

FIGURE 5

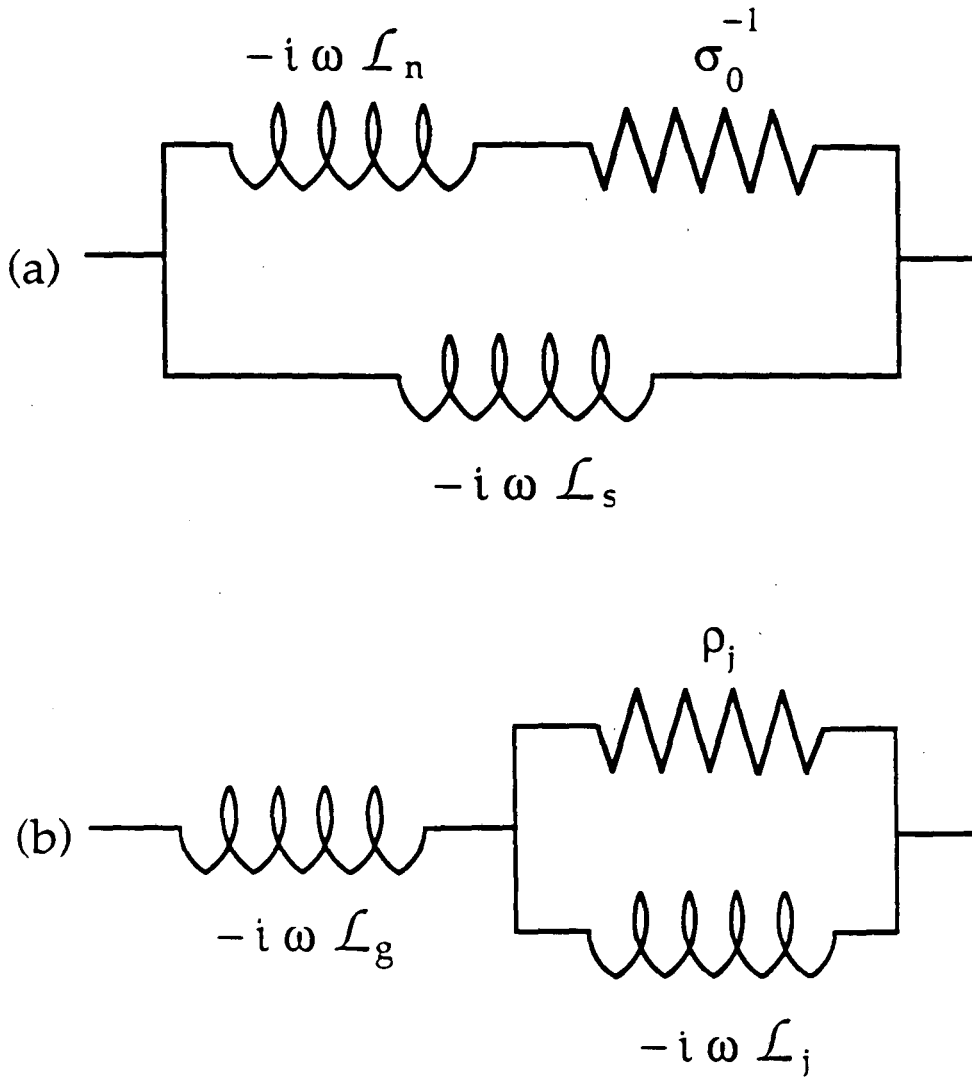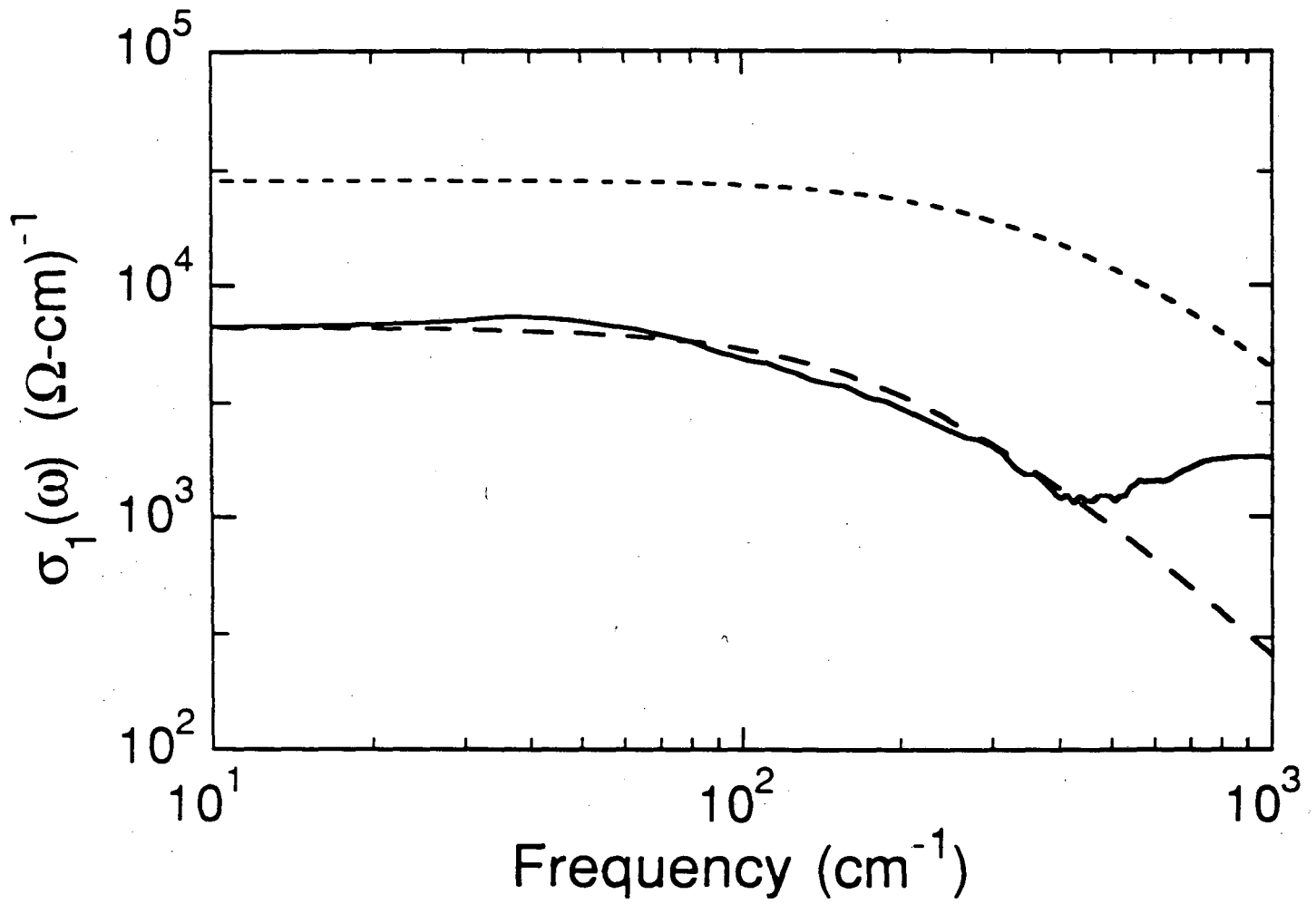XBL 919-2017

FIGURE 6

FIGURE 7

XBL 9110-2228

FIGURE 8

XBL 9110-2227

LAWRENCE BERKELEY LABORATORY
CENTER FOR ADVANCED MATERIALS
1 CYCLOTRON ROAD
BERKELEY, CALIFORNIA 94720